

Tunable shear thickening in active non-Brownian suspensions

Bhanu Prasad Bhowmik^{1,2,*} and Christopher Ness¹

¹*School of Engineering, University of Edinburgh, Edinburgh EH9 3JL, United Kingdom*

²*Department of Physics, Indian Institute of Science Education and Research Pune, Pune-411008, India.*

We study tunable shear thickening in active suspensions of non-Brownian, repulsive, frictional grains using particle-based simulation, finding that activity augments the rheology beyond the friction-mediated shear thickening paradigm. Specifically, increasing particle self-propulsion drives a viscosity-reducing ‘dethickening’ of the system at large stress, where the material would otherwise be in a thickened, highly viscous state. Self-propulsion introduces additional isotropic dynamics to the particles, which compete with the flow-driven formation of frictional contacts. The degree of dethickening can thus be tuned by varying a suitably-defined dimensionless active stress that quantifies this competition. Recognising the parallels between self-propulsion and other contemporary routes to dethickening, we demonstrate that our data obey a recently proposed scaling framework, supporting a universal description of the tunable rheology of dense suspensions.

Introduction. Flows of dense suspensions and slurries are frequently observed in industry and natural processes [1, 2]. One widespread rheological phenomena is shear thickening, where the relative viscosity of the suspension η_r increases with flow rate $\dot{\gamma}$ or applied stress σ [3–7]. There is a well-established consensus that this behaviour originates in the stress-mediated onset of frictional contacts between particles [8–11]. For a solid volume fraction ϕ sufficiently smaller than the jamming volume fraction ϕ_J , with increasing σ or $\dot{\gamma}$ the system exhibits a smooth transition between a low- η_r lubricated state, where repulsive forces separate particles, and a high- η_r frictional state. For ϕ close to ϕ_J the transition occurs abruptly with a discontinuous jump appearing in the constitutive curve $\eta_r(\dot{\gamma})$ [12–15].

Over the decades, shear thickening has drawn the attention of rheologists from both fundamental and applied domains. In the former, the difference between the microscopic phenomena of shear jamming and shear thickening has been studied. Recent work [13, 14, 16, 17] shows that, similar to shear jamming, shear thickening is associated with a critical transition but likely with different critical exponents. From the applied point of view, large increases in viscosity due to thickening can pose challenges in the flow of the suspensions such as pipe blockages and extreme sluggish flow of materials in food processing industries. Understanding and developing new ways to control, tune and exploit shear thickening behaviour is thus crucial and is beginning to receive much attention [18–23].

The key goal when addressing tunable shear thickening is to implement interventions that manipulate and, ideally, remove, the frictional contacts present at high σ or $\dot{\gamma}$ during flow. Although in practice this is typically approached as a formulation challenge, *i.e.* by adding surfactants or other molecules that control the physics of the particle-particle interactions [19, 20, 22, 24], recently several methods have been proposed to achieve this *on-the-fly*, that is, to impose a mechanical disturbance during flow that can affect the microstructure without chang-

ing the composition. This has been demonstrated by both orthogonal superposition (OSP) flow [21, 23] and by targeted use of vibrations [25, 26] or acoustic perturbations (AP) [27, 28]. In AP, the suspension is subjected to acoustic noise, which effectively introduces repulsive interactions among the particles [29–31] that prevent frictional contact formation. In the case of OSP, cyclic shear is applied orthogonal to the primary flow direction, that is, a flow in direction x and velocity gradient in y would be supplemented by oscillatory shear applied with flow along z and velocity gradient in y . Doing so, with sufficiently small amplitude, breaks the fragile load-bearing force network formed by simple shear alone, again preventing frictional contacts from forming. Interestingly, a recent study [32] suggests that the inclusion of a small number of active particles into an otherwise conventional shear thickening dense suspension can, dependent on the strength of activity, produce a low viscosity state even at large $\dot{\gamma}$. Analogous, perhaps, to the orthogonal cross shear mentioned above, the self-propulsion of the active particles contributes additional dynamics to the non-Brownian system that apparently disrupt the formation of a force chain network. By controlling the strength of activity, one can control the presence of frictional contacts and thus the viscosity. This observation suggests self-propulsion as a suitable candidate to achieve tunable shear thickening.

Here we use particle-based simulation, namely a variant of the discrete element method, to study tunable shear thickening of active dense suspensions of non-Brownian, frictional particles in the presence of repulsive interactions. The active particles are modelled as non-Brownian run-and-tumble particles [33–35], characterised by an active driving force f^a and a persistence time τ_p . We find that shear thickening can be tuned by varying the strength of the active forcing relative to the repulsive force acting between particles. The isotropic self-propelling motion of the active particles effectively prevents the formation of shear-induced force-chain networks and reduces the number of frictional contacts. We

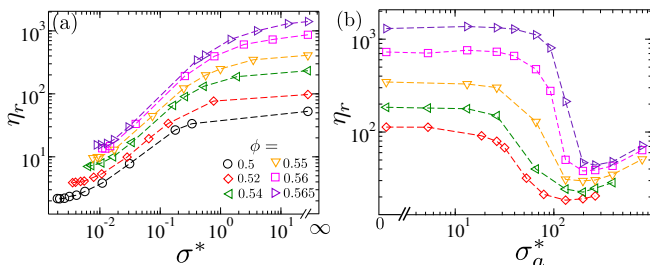


FIG. 1. Relative viscosity of an active shear thickening suspension. Shown are the variations of relative viscosity η_r as functions of (a) the dimensionless applied stress $\sigma^* = \sigma_{xy}a^2/f^r$ for fixed active stress $\sigma_a^* = 0$ and (b) the dimensionless active stress $\sigma_a^* = f^a/6\pi\eta_f\dot{\gamma}a^2$ for a range of volume fractions ϕ and for fixed applied stress $\sigma^* = 7.29$. The legend in (a) applies also to (b).

then compare this mechanism with the tunable shear thickening achieved by applying cyclic shear orthogonal to the primary flow direction, where force chains break due to the additional particle motion induced by the cyclic forcing. We show that tunable shear thickening with activity can be described using the same universal scaling framework proposed for cyclic perturbations, provided all parameters are mapped appropriately. Finally, we discuss how the discontinuous shear thickening and shear jamming region in the σ^* - ϕ phase diagram decreases in size with increasing activity strength.

Simulation details. We simulate $N = 10^3$ non-Brownian particles with Coulombic friction coefficient $\mu_p = 1$, suspended in a density ρ matched fluid of viscosity η_f . The particles have two different radii, a and $1.4a$, mixed in equal numbers and placed in a periodic, cubic box of length L . The rheological response is obtained by imposing a velocity profile $\mathbf{U}^\infty(y) = \dot{\gamma}y\hat{\mathbf{x}}$ to the suspending fluid phase, in the presence of Lees-Edwards boundary conditions across y . Here y is the distance along the direction of the velocity gradient and $\hat{\mathbf{x}}$ is the unit vector along the flow direction.

A particle with radius a_i located at position \mathbf{r} experiences a viscous drag force $\mathbf{f}_i^d = 6\pi\eta_f a_i (\mathbf{U}^\infty(r_y) - \mathbf{u}_i)$ and a torque $\boldsymbol{\tau}_i^d = 8\pi\eta_f a_i^3 (\boldsymbol{\Omega}^\infty - \boldsymbol{\omega}_i)$. Here \mathbf{u}_i and $\boldsymbol{\omega}_i$ are the linear and angular velocities of the particle, and $\boldsymbol{\Omega}^\infty = \frac{1}{2}(\nabla \times \mathbf{U}^\infty)$. Additionally, the relative velocity of a pair of particles $\mathbf{u}_{ij} = \mathbf{u}_j - \mathbf{u}_i$ is resisted by the viscous fluid, modelled here as short range hydrodynamic interactions [36–38]. The leading order term of this lubrication force is given by $\mathbf{f}_{ij}^h \sim \frac{\eta_f}{\delta_{ij}} (\mathbf{u}_{ij} \cdot \mathbf{n}_{ij}) \mathbf{n}_{ij}$, while that of the torque on the i^{th} particle due to the interaction with j^{th} particle is given by $\boldsymbol{\tau}_{ij}^h \sim \ln\left(\frac{a_i\eta_f}{\delta_{ij}}\right) (\mathbf{u}_{ij} \times \mathbf{n}_{ij})$. Here $\delta_{ij} = |\mathbf{r}_j - \mathbf{r}_i| - (a_i + a_j)$ is the separation between the particle surfaces, and $\mathbf{n}_{ij} = (\mathbf{r}_j - \mathbf{r}_i)/|\mathbf{r}_j - \mathbf{r}_i|$ is the center-to-center unit vector. We use $\delta_{ij} = 0.001a'$ in the force calculation whenever the measured $\delta_{ij} \leq 0.001a'$, allowing particles to come into direct contact. Here, a'

is the radius of the smaller particle. Additionally, we consider lubrication interactions only for pairs that have $\delta_{ij} < 0.5a'$, to reduce computational expense.

When $\delta_{ij} < 0$ the particles experience frictional contact forces, modelled as history dependent Hookean interactions. The normal component of the contact force is given by $\mathbf{f}_{ij}^{c,n} = -k_n\delta_{i,j}\mathbf{n}_{ij}$ and the tangential component is given by $\mathbf{f}_{ij}^{c,t} = -k_t\boldsymbol{\xi}_{i,j}$. Meanwhile the torque is given by $\boldsymbol{\tau}_{ij}^c = a_i (\mathbf{n}_{ij} \times \mathbf{f}_{ij}^{c,t})$. Here k_n and k_t are the normal and tangential stiffnesses, and $\boldsymbol{\xi}_{i,j}$ denotes the accumulated tangential displacement between particles, measured from the moment they first come into contact until the contact breaks. This displacement accounts for the history dependence of the frictional force [39]. Friction introduces an additional constraint into the system, preventing sliding between two particles when the ratio of their tangential to normal interaction force is less than the friction coefficient. Additionally, the particles repel each other via Coulombic interactions given by $\mathbf{f}_{ij}^r = -f^r e^{r_{ij}/r^*} \mathbf{n}_{ij}$ when $\delta_{ij} > 0$ and $-f^r e^{(a_i+a_j)/r^*} \mathbf{n}_{ij}$ for $\delta_{i,j} < 0$.

Finally, in addition to these interactions we introduce a randomly oriented force $\mathbf{f}_i^a = f^a \mathbf{e}_i$, applied independently on every particle to produce the self-propulsion, enforcing the constraint that $\sum_{i=1}^N \mathbf{f}_i^a = 0$ so that the center of mass does not drift. The orientation vector is constructed from discrete Cartesian components as $\mathbf{e} = f_x^a \hat{\mathbf{e}}_x + f_y^a \hat{\mathbf{e}}_y + f_z^a \hat{\mathbf{e}}_z$. Each component f_x^a , f_y^a , and f_z^a independently takes values from the discrete set $\{-1, 1\}$. After a persistence time interval τ_p , a new orientation is assigned by independently drawing the Cartesian components again from the same discrete distribution [35, 40]. Motivated by OSP results in which the dethickening effect is reported to saturate at large frequencies, we focus our exploration of the parameter space by setting $\tau_p \dot{\gamma} \sim 1$ throughout the following. We then define two dimensionless control parameters $\sigma^* = \sigma_{xy}a^2/f^r$ and $\sigma_a^* = f^a/6\pi\eta_f\dot{\gamma}a^2$ that compare, respectively, the hydrodynamic stress to the repulsive and active stresses. Here σ_{xy} is the shear stress measured in our simulations. Notably, we choose to construct these so that increasing σ^* leads to shear thickening whereas increasing σ_a^* leads to dethickening. (In practice this is achieved by varying f^r and f^a , having verified that our results are invariant under changes in $\dot{\gamma}$.)

Results. First we study systematically how the dimensionless stresses σ^* and σ_a^* control the viscosity. Fig. 1(a) shows the dependence of the relative viscosity $\eta_r = \sigma_{xy}/\dot{\gamma}\eta_f$ on σ^* for a range of solid volume fraction ϕ and a fixed value of $\sigma_a^* = 0$. The result reflects the standard behaviour of a shear thickening non-Brownian suspension of passive particles. Specifically, at small σ^* the particle interactions are lubrication dominated due to the repulsive force. As σ^* increases so does the number of direct mechanical contacts, resulting in a smooth

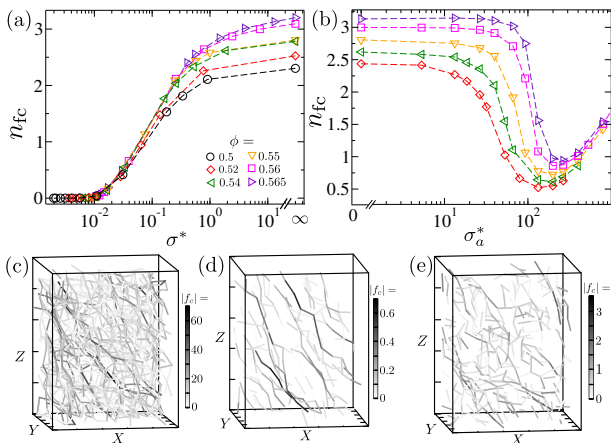


FIG. 2. Microstructure of an active shear thickening suspension. Shown are the variations of the mean number of frictional contacts n_{fc} as a function of (a) the dimensionless stress σ^* and (b) the dimensionless active stress σ_a^* . (c) Shows an example force chain network taken from a typical configuration with $\phi = 0.56$ in the steady state with $\sigma^* = \infty$ and $\sigma_a^* = 0$. (d) and (e) show the same as (c), but now with $\sigma^* = 0.02$, $\sigma_a^* = 0$, and $\sigma^* = 7.29$, $\sigma_a^* = 198.95$ respectively.

increase in viscosity. When σ^* exceeds a ϕ -dependent critical value, the applied stress overcomes the pairwise repulsive barrier set by f^r , leading to a rapid increase in η . The slope of the $\eta_r - \sigma^*$ curve increases with ϕ and approaches unity for the largest studied ϕ which indicates discontinuous shear thickening.

In Fig. 1(b) the equivalent dependence is shown for σ_a^* , measured at a fixed $\sigma^* = 7.29$. Here σ^* is large enough that the rheology is dominated by the frictional contacts for the passive system, thus producing a large, shear thickened, viscosity at $\sigma_a^* = 0$.

Now, as σ_a^* increases, the viscosity varies systematically. First, at small σ_a^* , the viscosity remains unchanged indicating that the strength of the self-propulsion stress is too low to affect the overall dynamics of the system. As σ_a^* increases, the viscosity decreases abruptly, primarily due to prevention of shear induced force chain formation as we will see in the next section. The viscosity then reaches a minimal value at a ϕ -dependent value of σ_a^* , beyond which there is then growth of η_r with σ_a^* . This trend remains for all the studied ϕ , with both the absolute and relative viscosity drops increasing as ϕ approaches ϕ_J . Overall the simulation data clearly show the opportunity for tunable shear thickening by varying σ_a^* , and raise the fundamental question of whether there is a microscopic connection between dethickening achieved using self-propulsion as done here, and by mechanical perturbation along the direction orthogonal to shear flow [23].

We next seek to understand the microstructural changes that take place in the presence of self-propulsion, and how these leads to tunable shear thickening. To do

so, we focus on the quantity n_{fc} , enumerating the number of frictional contacts per particle averaged over the system and representing the primary microscopic origin of the high viscosity state and jamming. The dependence of n_{fc} on σ^* and σ_a^* is shown in Fig. 2. As σ^* increases at $\sigma_a^* = 0$, n_{fc} increases smoothly from close to zero, its slope increasing modestly with increasing ϕ , Fig. 2(a). Again, this is consistent with the prevailing picture of shear thickening, in which frictional contacts become prevalent as a repulsive force is overcome at large stress. Meanwhile the dependence on σ_a^* follows the opposite trend, Fig. 2(b), suggesting a competition between the applied and active stresses. While the external driving leads to the proliferation of contacts by overcoming the repulsive barrier f_r , the self-propulsion reduces the number of contacts due to its additional isotropic motion, thus resulting in a low viscosity state at a ϕ which would otherwise be highly viscous. The evidence of such an effect is clear in the force chain network, shown in Figs. 2(c)–(e) for three different conditions, namely large (c) and small (d) σ^* in the absence of activity ($\sigma_a^* = 0$), and (e) with σ^* and σ_a^* both large. When the applied stress is strong and active stress is weak or absent, the particles come into mechanical contact and form anisotropic force chains that span the system as shown in Fig. 2(c). At small applied stress, the contacts are more lubricating with a smaller force scale, as shown by the colour map, however, still retain the highly anisotropic structure (Fig. 2(d)). Similarly, when the high active stress dominates, force chain network formation is prevented, leading to more isolated, pairwise contacts and consequently a lower viscosity (Fig. 2(e)).

Tunable shear thickening has been achieved previously by various methods. Two standard ones are the use of acoustic perturbation to the flowing samples, and applying oscillatory mechanical perturbation orthogonal to the primary flow direction. The acoustic perturbation can be understood by considering generation of effective repulsive potentials. In the case of orthogonal perturbation, the motion of the particles out of the shear plane reduces the number of frictional contacts, an effect that grows with the amplitude of the perturbation and oscillation frequency. Here the mean number of frictional contacts first decreases until a minimum value is achieved, before then increasing due to inertial motion [21, 23]. The additional dynamics of the particles due to cross shear is analogous to what we observe in our active system, the difference being that in one case the additional particle dynamics are due to external driving, whereas in the other they are due to self-propulsion. Direct comparison suggests that the amplitude of the active force f^a plays a similar role as the amplitude of the oscillation γ_{OSP} , while the persistence time τ_p has the same role as the oscillation frequency ω_{OSP} . Recent studies in active amorphous solids also suggest that cyclic shear and the presence of self-propelled particles with finite persistence

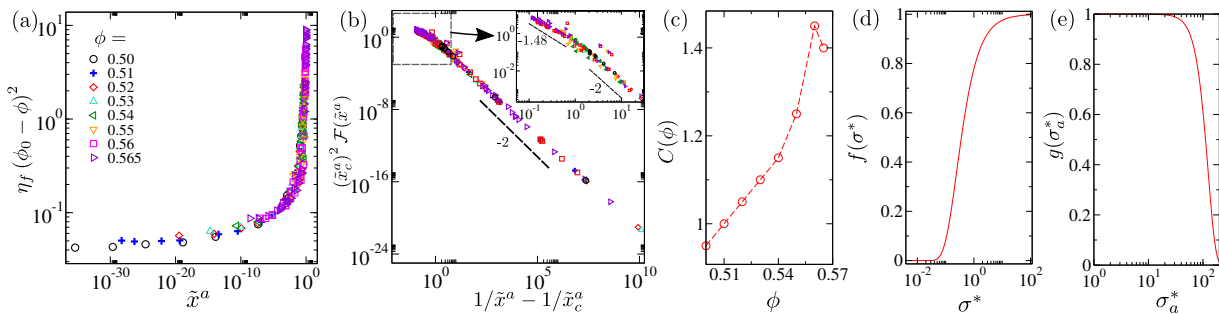


FIG. 3. Scaling of the rheology data for active shear thickening suspensions. Shown in (a) is a collapse of the data from Figs. 1(a) and (b) for a range of ϕ , σ^* and σ_a^* , onto a single master curve with the scaling variable for our active system being $\tilde{x}^a = f(\sigma^*)C(\phi)g(\sigma_a^*)/(\phi_0 - \phi)$. (b) Two power law regimes, with exponents -2 associated with isotropic jamming and exponent -1.48 (inset) associated with friction-dominated jamming. (c) Variation with volume fraction ϕ of the anisotropy factor $C(\phi)$; Sketches of the functional forms (d) $f(\sigma^*)$ and (e) $g(\sigma_a^*)$ used in the scaling variable for the data collapse.

time result in similar rheological responses [40, 41].

We further explore this analogy by testing the validity of a proposed scaling framework that seeks to describe universally the tunable shear thickening obtained under mechanical or acoustic forcing by collapsing the vast rheology data onto a single master curve. The scaling function in this data collapse shows a crossover between two critical points; a lubrication dominated divergence of viscosity at random close packing $\phi_0 \sim \phi_{\text{RCP}}$ to a friction dominated viscosity divergence at a lower volume fraction ϕ_J , as a function of a scaling variable defined as $\tilde{x} = f(\sigma)C(\phi)g(\dot{\Gamma})/(\phi_0 - \phi)$. Here, $C(\phi)$ is a so-called anisotropy factor first introduced in Ref. [13], which exhibits a nonmonotonic dependence on ϕ , with a maximum at an intermediate value. $\dot{\Gamma}$ is a dimensionless quantity defined as $\gamma_{\text{OSP}}\omega_{\text{OSP}}/\dot{\gamma}$. The functions $f(\sigma)$ and $g(\dot{\Gamma})$ take the form $f(\sigma) = e^{-(\sigma_0/\sigma)^{0.75}}$ and $g(\dot{\Gamma}) = e^{-(\dot{\Gamma}/\dot{\Gamma}_0)}$. The scaling relation is given by $\eta(\phi_0 - \phi)^2 = \mathcal{F}(\tilde{x})$. The scaling function $\mathcal{F}(\tilde{x})$ becomes a constant at small \tilde{x} , corresponding to the divergence of the viscosity at ϕ_0 with critical exponent 2 when the stress is low and interactions are lubrication dominated. $\mathcal{F}(\tilde{x})$ diverges at a critical value \tilde{x}_c corresponding to the friction dominated region occurring at high σ .

To implement this framework in our simulation setup, we first replace the variables σ by σ^* and $\dot{\Gamma}$ by σ_a^* , then define the scaling variable for the active system $\tilde{x}^a = f(\sigma^*)C(\phi)g(\sigma_a^*)/(\phi_0 - \phi)$. We then aim to collapse all our data for a large set of ϕ , σ^* and σ_a^* , as shown in Fig. 3(a). Doing so results in a reasonably good collapse of all the data for a large set of values of σ^* and σ_a^* , each for ϕ ranging from 0.5 to 0.565. We note that in the case of active systems we can have the same value of η_r for two different σ_a^* due to the nonmonotonicity reported in Fig. 1(b). In these cases we considered data only for those values of σ_a^* where the viscosity either remains constant or decreases with σ_a^* . Our scaling function looks the same as that found in Ref. [14], asymp-

totically approaching a constant value at small \tilde{x}^a and diverging at \tilde{x}_c^a . Fig. 3(b) shows the Cardy scaling [42], which manifests two different power law regimes. Here the exponent -2 corresponds to jamming at the isotropic jamming point ϕ_0 , while the exponent 1.48 corresponds to jamming due to friction dominated contacts at ϕ_J . The anisotropy factor $C(\phi)$ follows a largely monotonic growth with ϕ , Fig. 3(c), contrary to the values measured experimentally, whereas $f(\sigma^*)$ decreases following the form $e^{-0.25/\sigma^*}$ and $g(\sigma_a^*)$ decreases as $e^{-(\sigma_a^*/125)^{3.2}}$, Figs. 3(d)–(e). We note that the value of the obtained exponents is extremely sensitive to the value of \tilde{x}_c^a , likely true also of the values reported from experiments. Here we observe a sharp change in the exponent, ranging from 1.45 to 2.5, with only a small change in \tilde{x}_c^a . Moreover, the limited range of the power-law regime associated with the friction-dominated viscosity divergence makes it challenging to accurately determine \tilde{x}_c^a . Notably, the exponent associated with the friction-dominated viscosity divergence is close to that reported in Ref. [14]. Importantly, our system differs from the experimental system not least in that the frictional particles simulated here are modelled in a rather simplistic manner with several factors such as rolling friction and the hard-sphere limit not being taken into account.

Finally, we discuss how the presence of activity alters the size of the shear thickening and shear jamming regions in the $\sigma^* - \phi$ phase diagram, and thus offers a route to tuning the rheology. In a typical shear thickening system of frictional granular particles, when $\phi > \phi_0$ the system exhibits isotropic jamming for any finite value of σ^* as shown in red colour in Fig. 4. Below ϕ_0 , there is a region (shown in green in Fig. 4) where jamming occurs due to external shear when σ^* is above a certain $\phi(> \phi_J^\mu)$ dependent value. There also exists a region at smaller applied stress (gray in Fig. 4) where discontinuous shear thickening (DST) occurs. Following Ref. [14], we argue here that the boundary of the shear jamming region can be pushed towards isotropic jamming point with the help

of self-propulsion. The boundary is given by $\phi_J(\sigma^*, \sigma_a^*)$, which can be estimated from the critical value of the scaling variable $\tilde{x}_c^a = f(\sigma^*)C(\phi_J)g(\sigma_a^*)/(\phi_0 - \phi_J)$. Considering $C(\phi)$ a linear function $C(\phi) = 7.51\phi - 2.85$, we get

$$\phi_J(\sigma^*, \sigma_a^*) = \frac{\tilde{x}_c^a \phi_0 + 2.85g(\sigma_a^*)f(\sigma^*)}{(\tilde{x}_c^a + 7.51g(\sigma_a^*)f(\sigma^*))}. \quad (1)$$

Using Eq. 1 and the aforementioned functional form of $f(\sigma^*)$ and $g(\sigma_a^*)$, for a fixed σ_a^* , one can get the $\sigma^* - \phi_J$ line as shown by the green solid line in Fig. 4. As σ_a^* increases this line moves towards higher ϕ , indicating that shear jamming occurs at larger volume fraction in the presence of self-propulsion. This is supported by the finding of Ref. [32]. However, since our $\eta_r - \sigma_a^*$ exhibits nonmonotonic dependence at large σ_a^* , we are limited by a maximum practicable value of $\sigma_a^* \sim 150$. Here the shear jamming region is considerably smaller than the activity-free case (Fig. 4(b)), but unlike Ref. [14] it does not vanish. (Though earlier experiments do support a saturation of viscosity reduction under strong cross shear [21].)

We can similarly estimate how the DST region alters with active stress. This region is given by the condition $\frac{d \ln \eta_r}{d \ln \sigma^*} > 1$. Using the scaling relation $\eta_r(\phi - \phi_0)^2 = \mathcal{F}(\tilde{x}^a)$ with $\tilde{x}^a = f(\sigma^*)C(\phi)g(\sigma_a^*)/(\phi_0 - \phi)$, we get

$$\frac{\sigma^*}{\mathcal{F}(\tilde{x}^a)} \frac{d\mathcal{F}(\tilde{x}^a)}{d\tilde{x}^a} \frac{df(\sigma^*)}{d\sigma^*} \frac{C(\phi)g(\sigma_a^*)}{\phi_0 - \phi} > 1. \quad (2)$$

For large \tilde{x}^a , considering $\mathcal{F}(\tilde{x}^a) = (\tilde{x}_c^a - \tilde{x}^a)^{-\delta}$, we get

$$\frac{-\delta\sigma^*}{(\tilde{x}_c^a - \tilde{x}^a)} \frac{df(\sigma^*)}{d\sigma^*} \frac{C(\phi)g(\sigma_a^*)}{\phi_0 - \phi} > 1. \quad (3)$$

Now, for a fixed σ^* , as σ_a^* increases $g(\sigma_a^*)$ decreases, which forces a decrease in $\phi_0 - \phi$ to satisfy the inequality in Eq. 3. Thus with increasing active stress the boundary of the DST region moves towards ϕ_0 . However, similar to shear jamming region, unlike OSP in Ref. [14], this shear thickening region will not vanish since we cannot push to the limit $g(\sigma_a^*) = 0$ by making $\sigma_a^* \rightarrow 0$ since the viscosity starts increasing as we cross certain values of active stress due to activity induced diffusion. Quantitatively the phase boundary of the DST region (gray dashed line in Fig. 4) is given by

$$\frac{-\delta\sigma^*}{(\tilde{x}_c^a - \tilde{x}^a)} \frac{df(\sigma^*)}{d\sigma^*} \frac{C(\phi)g(\sigma_a^*)}{\phi_0 - \phi} = 1, \quad (4)$$

and can be estimated for a fixed σ_a^* using the functional form of $f(\sigma^*)$ and $g(\sigma_a^*)$. Fig. 4(b) shows the shear thickening region for a very large $\sigma_a^* = 150$.

Conclusion. We have studied tunable shear thickening in active dense suspensions of non-Brownian particles. The degree of shear thickening can be tuned by varying a dimensionless active stress which characterises the ratio of the active stress to the stress due to external driving. Self-propulsion of the particles reduces the

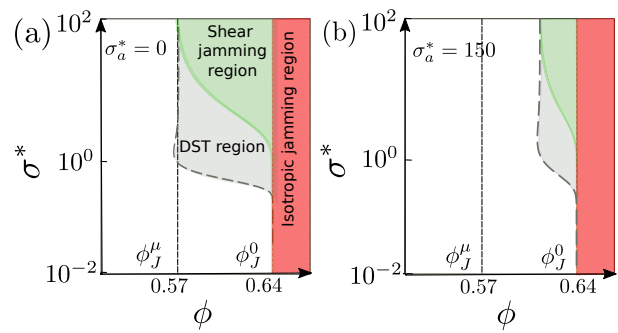


FIG. 4. Tuning of the shear jamming and discontinuous shear thickening (DST) regions due to active stress. (a) Isotropic jamming (red), shear jamming (green), and DST (gray) regions in the $\sigma^* - \phi$ phase diagram in the absence of activity, with $\sigma_a^* = 0$. (b) Altered shear jamming and DST regions under a large active stress, $\sigma_a^* = 150$.

number of frictional contacts, similar to the mechanism observed in tunable shear thickening achieved by applying cyclic shear orthogonal to the primary flow direction. A scaling framework that describes tunable shear thickening in the presence of OSP is used to explain the tunable shear thickening induced by self-propulsion, leading to a successful collapse that supports this perspective as a unifying tool for suspension rheology. Our study is conducted by varying the active force at a fixed persistence time; therefore, the persistence time does not appear in the scaling variables. However, we note that tunable shear thickening can also be achieved by varying the persistence time, and indeed this may allow further optimisation of the $\sigma^* - \phi$ phase diagram, possibly eliminating the DST and shear jamming regions entirely. In such cases, the scaling variables would need to be modified accordingly, and this will be studied in future work.

Acknowledgement. BPB acknowledges support from the INSPIRE Faculty Fellowship by Department of Science and Technology (DST), Government of India. We thank Anna Barth and Itai Cohen for discussions.

* bhowmikbhanuprasad592@gmail.com

- [1] E. Guazzelli and O. Pouliquen, Rheology of dense granular suspensions, *Journal of Fluid Mechanics* **852**, 10.1017/jfm.2018.548 (2018).
- [2] C. Ness, R. Seto, and R. Mari, The physics of dense suspensions, *Annual Review of Condensed Matter Physics* **13**, 97 (2022).
- [3] A. B. Metzner and M. Whitlock, Flow behavior of concentrated (dilatant) suspensions, *Transactions of The Society of Rheology* **2**, 239 (1958).
- [4] H. A. Barnes, Shear-thickening (“dilatancy”) in suspensions of nonaggregating solid particles dispersed in Newtonian liquids, *Journal of Rheology* **33**, 329 (1989).

- [5] J. Bender and N. J. Wagner, Reversible shear thickening in monodisperse and bidisperse colloidal dispersions, *Journal of Rheology* **40**, 899 (1996).
- [6] J. R. Melrose and R. C. Ball, Continuous shear thickening transitions in model concentrated colloids—the role of interparticle forces, *Journal of Rheology* **48**, 937 (2004).
- [7] E. Brown, N. A. Forman, C. S. Orellana, H. Zhang, B. W. Maynor, D. E. Betts, J. M. DeSimone, and H. M. Jaeger, Generality of shear thickening in dense suspensions, *Nature Materials* **9**, 220 (2010).
- [8] R. Seto, R. Mari, J. F. Morris, and M. M. Denn, Discontinuous shear thickening of frictional hard-sphere suspensions, *Physical Review Letters* **111**, 218301 (2013).
- [9] R. Mari, R. Seto, J. F. Morris, and M. M. Denn, Shear thickening, frictionless and frictional rheologies in non-brownian suspensions, *Journal of Rheology* **58**, 1693 (2014).
- [10] R. Mari, R. Seto, J. F. Morris, and M. M. Denn, Discontinuous shear thickening in brownian suspensions by dynamic simulation, *Proceedings of the National Academy of Sciences* **112**, 15326 (2015).
- [11] A. Singh, R. Mari, M. M. Denn, and J. F. Morris, A constitutive model for simple shear of dense frictional suspensions, *Journal of Rheology* **62**, 457 (2018).
- [12] M. Wyart and M. E. Cates, Discontinuous shear thickening without inertia in dense non-brownian suspensions, *Physical Review Letters* **112**, 098302 (2014).
- [13] M. Ramaswamy, I. Griniasty, D. B. Liarte, A. Shetty, E. Katifori, E. Del Gado, J. P. Sethna, B. Chakraborty, and I. Cohen, Universal scaling of shear thickening transitions, *Journal of Rheology* **67**, 1189 (2023).
- [14] M. Ramaswamy, I. Griniasty, J. P. Sethna, B. Chakraborty, and I. Cohen, Universal scaling framework for controlling phase behavior in thickening and jamming suspensions, *Physical Review Letters* **134**, 058203 (2025).
- [15] A. R. Barth, N. Singh, S. J. Thornton, P. Kakhandiki, E. Y. X. Ong, M. Ramaswamy, A. M. Shetty, B. Chakraborty, J. P. Sethna, and I. Cohen, Acoustic tuning of shear thickening suspensions: A universal scaling analysis, *Journal of Rheology* **70**, 419 (2026).
- [16] M. Wyart and M. E. Cates, Discontinuous shear thickening without inertia in dense non-brownian suspensions, *Phys. Rev. Lett.* **112**, 098302 (2014).
- [17] N. Malbranche, A. Santra, B. Chakraborty, and J. F. Morris, Scaling analysis of shear thickening suspensions, *Frontiers in Physics* **Volume 10 - 2022**, 10.3389/fphy.2022.946221 (2022).
- [18] F. Blanc, E. Lemaire, and F. Peters, Tunable fall velocity of a dense ball in oscillatory cross-sheared concentrated suspensions, *Journal of Fluid Mechanics* **746**, R4 (2014).
- [19] P. Bourrienne, V. Niggel, G. Polly, T. Divoux, and G. H. McKinley, Tuning the shear thickening of suspensions through surface roughness and physico-chemical interactions, *Physical Review Research* **4**, 033062 (2022).
- [20] C.-P. Hsu, S. N. Ramakrishna, M. Zanini, N. D. Spencer, and L. Isa, Roughness-dependent tribology effects on discontinuous shear thickening, *Proceedings of the National Academy of Sciences* **115**, 5117 (2018).
- [21] N. Y. Lin, C. Ness, M. E. Cates, J. Sun, and I. Cohen, Tunable shear thickening in suspensions, *Proceedings of the National Academy of Sciences* **113**, 10774 (2016).
- [22] N. M. James, C.-P. Hsu, N. D. Spencer, H. M. Jaeger, and L. Isa, Tuning interparticle hydrogen bonding in shear-jamming suspensions: Kinetic effects and consequences for tribology and rheology, *The Journal of Physical Chemistry Letters* **10**, 1663 (2019).
- [23] C. Ness, R. Mari, and M. E. Cates, Shaken and stirred: Random organization reduces viscosity and dissipation in granular suspensions, *Science Advances* **4**, eaar3296 (2018).
- [24] N. Fernandez, R. Mani, D. Rinaldi, D. Kadau, M. Mosquet, H. Lombois-Burger, J. Cayer-Barrioz, H. J. Herrmann, N. D. Spencer, and L. Isa, Microscopic mechanism for shear thickening of non-brownian suspensions, *Physical Review Letters* **111**, 108301 (2013).
- [25] C. Hanotin, S. Kiesgen de Richter, P. Marchal, L. J. Michot, and C. Baravian, Vibration-induced liquefaction of granular suspensions, *Physical Review Letters* **108**, 198301 (2012).
- [26] C. Garat, S. Kiesgen de Richter, P. Lidon, A. Colin, and G. Ovarlez, Using good vibrations: Melting and controlled shear jamming of dense granular suspensions, *Journal of Rheology* **66**, 237 (2022).
- [27] P. Sehgal, M. Ramaswamy, I. Cohen, and B. J. Kirby, Using acoustic perturbations to dynamically tune shear thickening in colloidal suspensions, *Physical Review Letters* **123**, 128001 (2019).
- [28] P. Sehgal, M. Ramaswamy, E. Y. X. Ong, C. Ness, I. Cohen, and B. J. Kirby, Programmable viscosity metamaterials: Designing fluid properties using temporal superposition of shear and acoustics, *Physical Review Research* **6**, 043107 (2024).
- [29] M. Settnes and H. Bruus, Forces acting on a small particle in an acoustical field in a viscous fluid, *Physical Review E* **85**, 016327 (2012).
- [30] P. B. Muller, M. Rossi, A. G. Marin, R. Barnkob, P. Augustsson, T. Laurell, C. J. Kahler, and H. Bruus, Ultrasound-induced acoustophoretic motion of microparticles in three dimensions, *Physical Review E* **88**, 023006 (2013).
- [31] D. J. Collins, R. O’Rourke, C. Devendran, Z. Ma, J. Han, A. Neild, and Y. Ai, Self-aligned acoustofluidic particle focusing and patterning in microfluidic channels from channel-based acoustic waveguides, *Physical Review Letters* **120**, 074502 (2018).
- [32] B. P. Bhowmik, Tuning the viscosity and jamming point in dense active non-brownian suspensions, *arXiv* (2025), 2506.13316 [cond-mat.soft].
- [33] H. M. Lopez, J. Gachelin, C. Douarche, H. Auradou, and E. Clement, Turning bacteria suspensions into superfluids, *Physical Review Letters* **115**, 028301 (2015).
- [34] E. Clement, A. Lindner, C. Douarche, and H. Auradou, Bacterial suspensions under flow, *The European Physical Journal Special Topics* **225**, 2389 (2016).
- [35] R. Mandal, P. J. Bhuyan, M. Rao, and C. Dasgupta, Active fluidization in dense glassy systems, *Soft Matter* **12**, 6268 (2016).
- [36] D. J. Jeffrey and Y. Onishi, Calculation of the resistance and mobility functions for two unequal rigid spheres in low-reynolds-number flow, *Journal of Fluid Mechanics* **139**, 261–290 (1984).
- [37] S. Kim and S. Karrila, *Microhydrodynamics: Principles and Selected Applications*, Butterworth - Heinemann series in chemical engineering (Dover Publications, 2005).
- [38] O. Cheal and C. Ness, Rheology of dense granular suspensions under extensional flow, *Journal of Rheology* **62**, 501 (2018).

- [39] P. A. Cundall and O. D. L. Strack, A discrete numerical model for granular assemblies, *Géotechnique* **29**, 47 (1979).
- [40] R. Sharma and S. Karmakar, Activity-induced annealing leads to a ductile-to-brittle transition in amorphous solids, *Nature Physics* **21**, 253 (2025).
- [41] Y. Goswami, G. V. Shivashankar, and S. Sastry, Yielding behaviour of active particles in bulk and in confinement, *Nature Physics* **21**, 817 (2025).
- [42] J. Cardy, *Scaling and Renormalization in Statistical Physics*, Vol. 5 (Cambridge University Press, Cambridge, 1996).